Technical Notes

Nonintrusive Freestream Velocity Measurement in a Large-Scale Hypersonic Wind Tunnel

M. A. Mustafa* and N. J. Parziale†
Stevens Institute of Technology, Hoboken, New Jersey 07030
and
M. S. Smith‡ and E. C. Marineau§
Arnold Engineering Development Complex, White Oak, Silver Spring, Maryland 20903

DOI: 10.2514/1.J056177

I. Introduction

HIGH-SPEED wind tunnels typically rely on pressure and/or temperature measurement and nozzle-flow calculations to determine the freestream conditions. This practice can require a complex treatment of the thermochemical state of the gas. The calorically perfect gas assumption begins to break down when producing air or N_2 flows from a stagnated reservoir to freestream Mach number $M_\infty > 6$. Rapid expansion in the nozzle can require modeling thermodynamic nonequilibrium processes, and if the gas is stagnated to high enthalpy, nonequilibrium chemistry must also be considered [1]. Moreover, an excluded-volume equation of state may need to be used for high reservoir densities [2,3]. Although the modeling framework of these flows is tractable, some of the fundamentals pertaining to the thermochemical rate processes continue to be an ongoing topic of research [1].

One means of validating these run condition and nozzle-flow calculations is direct measurement in the freestream. Particle-based methods of velocimetry, such as particle image velocimetry, can produce high-quality multicomponent velocity data [4]. However, the engineering challenges associated with implementing particle-based techniques in large-scale high-speed facilities include timing, particle-seeding density and uniformity, and minimizing flow disturbances when injecting particles [5]. More importantly, there is the fundamental limitation of reduced particle response at Knudsen and Reynolds numbers [6] typical of high-speed wind tunnels, which can compromise the resolution of fine time and length scales.

In contrast to the limitations of particle-based techniques, implementation of tagging velocimetry is not constrained by the aforementioned issues in large-scale high-speed facilities. Noted methods and tracers of tagging velocimetry include VENOM [7], APART [8], RELIEF [9], FLEET [10], STARFLEET [11], PLEET [12], nitrogen oxides [13–15], iodine [16], acetone [17], and the hydroxyl group techniques [18–21]. Continually advancing laser and imaging technology has enabled tagging velocimetry to be used in large-scale facilities where other approaches are difficult to implement.

This technical note reports the direct measurement of freestream-velocity profiles in AEDC Hypervelocity Tunnel 9 (Tunnel 9) with krypton tagging velocimetry (KTV). The KTV experimental setup is described, followed by an explanation of Tunnel 9 and the conventional method of run-condition calculation. KTV exposures are presented for four different Tunnel 9 conditions. Then, for two conditions, instantaneous velocity profiles and a comparison of the freestream velocity as calculated by conventional methods and KTV are presented.

II. Krypton Tagging Velocimetry Setup

Krypton tagging velocimetry (KTV), relative to other tagging velocimetry techniques, relies on a chemically inert tracer and does not require significantly altering the local thermochemical state of the gas. This property may enable KTV to broaden the utility of tagging velocimetry because the technique can be applied in gas flows where the chemical composition is difficult to prescribe or predict. The technique currently requires two pulsed tunable lasers and one intensified camera. Using metastable noble gas as a tagging velocimetry tracer was first suggested by Mills et al. [22] and Balla and Everheart [23]. KTV was first demonstrated by Parziale et al. [24,25] to measure the velocity along the centerline of an underexpanded jet of N_2/Kr mixtures. Following that work, Zahradka et al. [26,27] used KTV to make measurements of the mean and fluctuating profiles in a Mach 2.7, 99% N_2/1% Kr turbulent boundary layer. Recently, Mustafa et al. [28] used KTV to measure seven simultaneous profiles of streamwise velocity and velocity fluctuations in the incoming boundary layer and immediately upstream of a 24 deg compression corner in a $M_\infty = 2.8$, $Re_\Theta = 1750$, 99% N_2/1% Kr shock-wave/turbulent-boundary-layer interaction.

Following the energy level diagram (Racah nl$[K]_J$ notation) in Fig. 1, KTV is performed as follows.

1) Seed a base flow with krypton globally.

2) Write step. Photosynthesize the write line and metastable krypton tracer with a pulsed-tunable laser: two-photon excitation of $4p^6(^1S_0) \rightarrow 5p[3/2]_2$ (214.7 nm) and rapid decay to resonance state $5p[3/2]_2 \rightarrow 5s[3/2]_1^\circ$ (819.0 nm) and metastable state $5p[3/2]_2 \rightarrow 5s[3/2]_2^\circ$ (760.2 nm). We image the $5p[3/2]_2 \rightarrow 5s[3/2]_1^\circ$ (819.0 nm) transitions with a camera positioned normal to the flow. This process takes approximately 50 ns [29] and comprises the "write line".

3) Read step. Record the displacement of the tagged metastable krypton by imaging the laser-induced fluorescence that is produced with an additional pulsed-tunable laser: excite $5p[3/2]_1$ level by $5s[3/2]_2^\circ \rightarrow 5p[3/2]_1$ transition with laser sheet (769.5 nm) and read spontaneous emission of $5p[3/2]_1 \rightarrow 5s[3/2]_1^\circ$ (829.8 nm) transitions with a camera positioned normal to the flow. This process takes approximately 50 ns [29] and comprises the "read line". We choose a different energy level for the read step as opposed to previous KTV work [24–28] because of higher observed signal-to-noise ratio (SNR) when performing the write/read steps in a stationary krypton cell. A fluorescence model that characterizes the SNR of the KTV technique with different read excitations is forthcoming and not included in this note.

The experiment was run using two tunable lasers to provide the 214.7 nm (write) and 769.5 nm (read) laser beams required for KTV. The write laser consisted of a frequency-doubled Quanta Ray Pro-350 Nd:YAG laser and a frequency-tripled Sirah PrecisionScan Dye Laser. The Nd:YAG laser pumped the dye laser with 1000 mJ/pulse at a wavelength of 532 nm. The dye in the laser was DCM with a dimethyl sulfoxide (DMSO) solvent, and the laser was

Received 24 March 2017; accepted for publication 12 July 2017; published online 25 August 2017.

*Graduate Student, Mechanical Engineering, Castle Point on Hudson. Student Member AIAA.
†Assistant Professor, Mechanical Engineering, Castle Point on Hudson. Member AIAA.
‡Senior Research Engineer, National Aerospace Solutions, Silver Spring, MD 20903. Senior Member AIAA.
§Chief Technologist. Senior Member AIAA.

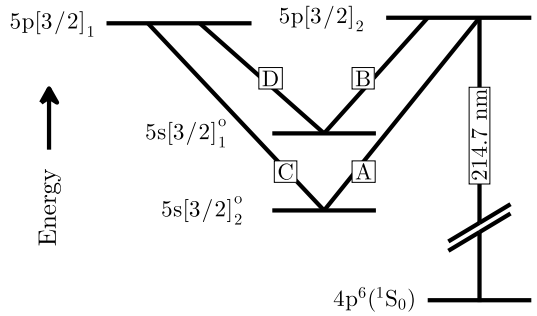

Fig. 1 Energy diagram for KTV. Racah nl[K]$_J$ notation. A is 760.2 nm, B is 819.0 nm, C is 769.5 nm, and D is 829.8 nm.

tuned to output a 644.1 nm beam. Frequency tripling of the dye-laser output was performed using Sirah tripling optics (THU 205).

The write-laser beam setup can result in approximately 10–13 mJ/pulse; however, approximately 3 mJ was used for this experiment by reducing the Nd:YAG pump-laser power. The wavelength was 214.7 nm, with a linewidth of approximately 0.045 cm^{-1}, a pulse width of approximately 7 ns, and a repetition rate of 10 Hz. The write-laser beam was directed into the test section with 1 in. fifth-harmonic Nd:YAG laser mirrors (IDEX Y5-1025-45) and focused into the test section with a 1500 mm fused-silica lens to form a line in the spanwise direction. Assuming Gaussian beam propagation, the beam-waist diameter and fluence are approximately 80 μm and 30 J/cm^2, respectively.

The read laser consisted of a frequency-doubled Quanta Ray Pro-350 Nd:YAG laser and a Sirah PrecisionScan Dye Laser. The Nd:YAG laser pumped the dye laser with 500 mJ/pulse at a wavelength of 532 nm. The dye in the laser was Styryl 8 with a DMSO solvent, and the laser was tuned to output a 769.5 nm beam.

The read-laser beam setup resulted in approximately 30 mJ/pulse, with a wavelength of 769.5 nm, a linewidth of approximately 0.025 cm^{-1}, a pulse width of approximately 7 ns, and a repetition rate of 10 Hz. The read-laser beam was directed into the test section using 2 in. broadband dielectric mirrors (Thorlabs BB2-E02) and focused to a sheet of ≈1000 μm × 25 mm with a 2000 mm fused silica cylindrical lens. This "read sheet" reexcites the metastable Kr tracer atoms so that their displacement can be measured.

The laser and camera timing are controlled by a pulse-delay generator (SRS DG645). The intensified camera used for all experiments is a 16-bit Princeton Instruments PIMAX-4 1024 × 1024 with an 18 mm grade 1, Gen III extended red filmless intensifier with P46 phosphor (PM4-1024i-HR-FG-18-P46-CM). The gain is set to 100% with 2 × 1 (spanwise × streamwise) pixel binning to ensure a 10 Hz frame rate. The prime lens used is an AF-S NIKKOR 200 mm $f/2G$ ED-VR-II and positioned approximately 1.1 m from the write/read location, which was at the center of the test cell. A Nikon PK-13 27.5 mm extension tube was inserted between the lens and the F/C adapter to reduce the minimum focal distance and increase the magnification of the lens. Two high-precision 800 nm long-pass filters (Thorlabs FELH0800, transmission of 3.5e–4% at the read-laser wavelength of 769.5 nm) are placed in series between the lens and the intensifier to minimize the noise resulting from the read-laser pulse reflection and scatter from solid surfaces. The dual-image feature was used, and the camera gate was opened for 50 ns immediately following the write-laser pulse to capture the spontaneous emission of $5p[3/2]_2 \rightarrow 5s[3/2]_1^\circ$ (819.0 nm) transitions. Then, 2 μs later, the camera gate was opened for 50 ns immediately following the read-laser pulse to capture the spontaneous emission of $5p[3/2]_1 \rightarrow 5s[3/2]_1^\circ$ (829.8 nm) transitions.

III. Experimental Facility and Run Condition Calculations

The experiments were conducted in the Arnold Engineering Development Complex (AEDC) Hypervelocity Wind Tunnel Number 9 (Tunnel 9) shown in Fig. 2. Tunnel 9 is a hypersonic, nitrogen-gas, blowdown wind tunnel with interchangeable nozzles that allow for testing at Mach numbers of 7, 8, 10, and 14 over a unit Reynolds number range of 1.77e6 to 158.8e6 1/m. The test section is a 1.52-m-diam (5-ft-diam), 3.66-m-long (12-ft-long) cell that enables testing of large-scale model configurations. More details pertaining to the facility can be found in Marren and Lafferty [30].

The nominal run conditions for this test series, as calculated by the staff at AEDC (conventional method), are found in Table 1. The reservoir pressure, reservoir temperature, and pitot pressure are measured. Reservoir enthalpy and reservoir entropy are determined using the measured reservoir conditions and the data from a Mollier diagram for equilibrium N_2. The freestream conditions are calculated from the reservoir conditions and pitot pressure using a procedure that assumes an isentropic nozzle expansion. The procedure is initiated with an initial estimate for the freestream Mach number. Using the estimated freestream Mach number and measured pitot pressure, freestream pressure is obtained from the Rayleigh pitot formula. In addition, it is assumed that the degree of vibrational excitation at the nozzle exit is negligible, and so the ratio of specific heats is equal to 7/5. The freestream temperature (and freestream sound-speed) is calculated using the freestream pressure and reservoir entropy. Then, freestream velocity is obtained based on the conservation of reservoir enthalpy. This value of velocity is converted to Mach number and is compared to the initial estimated Mach number value. When these two agree to within a specified tolerance, the calculation is complete and the tunnel conditions are known.

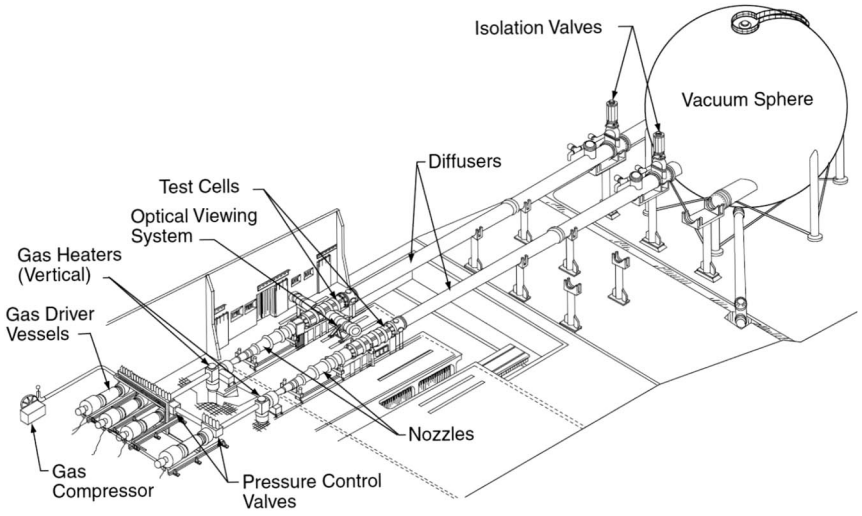

Fig. 2 Annotated AEDC Hypervelocity Tunnel 9 schematic. Two legs are shown; the upper leg was used for this project.

Table 1 Nominal run conditions for current test series as determined by conventional methods; M_∞, Re_∞^{unit}, U_∞, ρ_∞, and T_∞ are the freestream Mach number, unit Reynolds number, velocity, density, and temperature; h_R and P_R are the reservoir enthalpy and pressure

Condition	M_∞	Re_∞^{unit}, 1/m	U_∞, km/s	ρ_∞, kg/m^3	T_∞, K	P_R, MPa	h_R, MJ/kg
A	13.2	1.65	1.92	3.04e–3	50.9	14.6	1.90
B	9.44	1.88	1.37	4.85e–3	50.7	2.16	1.00
C	9.82	13.1	1.43	3.26e–2	51.1	18.2	1.08
D	10.0	30.3	1.47	7.44e–2	51.9	44.8	1.14

IV. Implementation of Krypton Tagging Velocimetry in Tunnel 9

KTV is implemented in Tunnel 9 by doping the N_2 flow with 1% Kr by mole fraction in the reservoir. A predetermined mass of Kr is injected into the "gas heaters" pictured in Fig. 2 following the N_2 "blowoff". The blowoff refers to when the heating vessel is checked for vacuum and flushed with 1 atm of N_2. Then, the typical high-pressure N_2 filling procedure continues unchanged from normal operation. It is assumed that the 99% N_2/1% Kr mixture becomes well mixed by the turbulent, high-pressure N_2 injection and subsequent high-temperature reservoir-heating process.

The concentration of krypton in the flow is dilute, and so the thermophysical properties of the flow are nominally unchanged from normal operation. The effect of krypton seeding on the transport properties is calculated using Cantera [31] via the semi-empirical Chapman–Enskog method [32] with the appropriate thermodynamic data [33]. For example, seeding N_2 with 1% Kr mole fraction alters the Mach, Reynolds, Prandtl, and Peclet numbers and the ratio of specific heats by ≈0.1–0.3%.

V. Results

In this section, we present KTV exposures for four different Tunnel 9 conditions (listed in Table 1). Then, for two conditions, instantaneous velocity profiles and a comparison of the freestream velocity as calculated by conventional methods and KTV are presented. The purpose of this effort was to explore the range of conditions over which KTV could deliver results with sufficient SNR; in this study, the conditions span a range of $M_\infty = 9.4$–13.2 and $Re_\infty^{\text{unit}} = 1.6$–30 m^{-1}.

The write and read exposures are recorded separately with the interline feature of the intensified camera with a delay of 2 μs. We present a composite of the write/read exposures for all four conditions as Figs. 3, 4. The Mach 14 exposure (Fig. 3, left) was the first measurement attempted, and so as a conservative first approach, the digitizer was set to its slowest speed, 4 MHz (lowest noise level). This was done to achieve the highest possible SNR while still yielding a 25-mm-tall measurement window, which was a minimum requirement for the test to be considered a success. In subsequent experiments, the camera digitizer was set to its highest speed 32 MHz (highest noise level) because the SNR was deemed sufficient and so the field of view was enlarged.

To process the KTV exposures in Figs. 3 and 4, the line centers were found in the following way.

1) Crop the image to an appropriate field of view.

2) Apply a two-dimensional Wiener adaptive-noise-removal filter.

3) Convert the images to double precision numbers and normalize the intensity to fall in the range of 0–1.

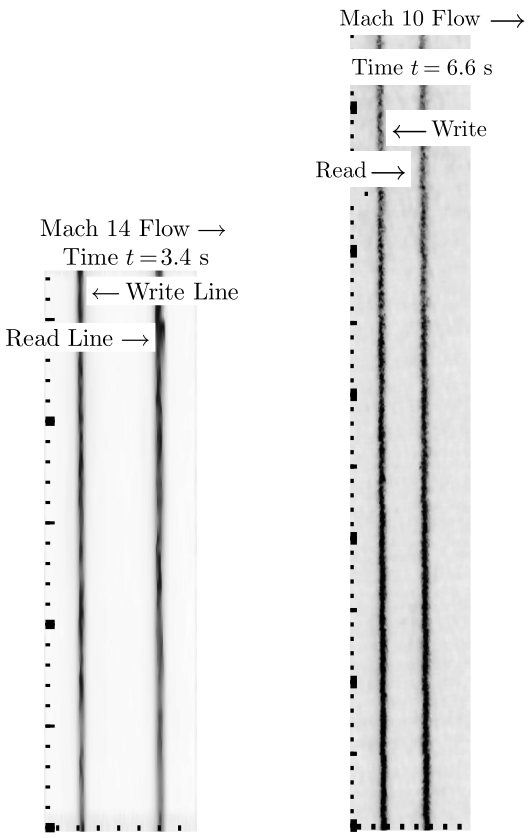

Fig. 3 Time stamp denotes tunnel starting trigger. Composite of write and read KTV exposures from Tunnel 9 condition A (left) and condition B (right). Conditions in Table 1. Tick marks denote millimeters. Inverted intensity scale. Write/read delay of 2 μs.

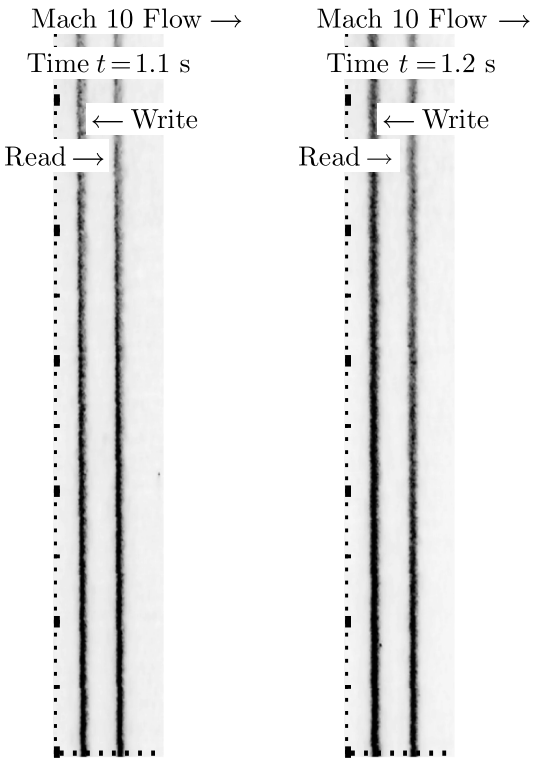

Fig. 4 Time stamp denotes tunnel starting trigger. Composite of write and read KTV exposures from Tunnel 9 condition C (left) and condition D (right). Conditions in Table 1. Tick marks denote millimeters. Inverted intensity scale. Write/read delay of 2 μs.

4) Apply the Gaussian peak finding algorithm from O'Haver [34] to find the line centers for the top row using the write and read lines in the top row of each image as a first guess.

5) Proceeding from the top down, apply the Gaussian peak finding algorithm from O'Haver [34] to find the line centers for each row using the line center location immediately above as the guess.

Steps 4 and 5 are done in parallel in MATLAB for the exposures for each run. The freestream-velocity profiles are presented for conditions A and B in Figs. 5 and 6, respectively. Error bars for the KTV measurements are calculated as

$$\delta U_{\mathrm{KTV}} = \left[\left(\delta\Delta x \frac{\partial U}{\partial \Delta x}\right)^2 + \left(\delta\Delta t \frac{\partial U}{\partial \Delta t}\right)^2 + \left(v'_{\mathrm{RMS}} \frac{\mathrm{d}U}{\mathrm{d}y}\Delta t\right)^2\right]^{1/2} \quad (1)$$

The uncertainty in the measured displacement distance, Δx, of the metastable tracer is estimated as the 95% confidence bound on the write and read locations from the Gaussian fits. The uncertainty Δt is estimated to be 50 ns, primarily due to fluorescence blurring as considered in Bathel et al. [35]. From the manufacturer's specification, we estimate that the timing jitter is relatively small, approximately 1 ns for each laser. The fluorescence blurring primarily occurs because of the time scale associated with the $5p[3/2]_2 \rightarrow 5s[3/2]_1^\circ$ and $5p[3/2]_1 \rightarrow 5s[3/2]_1^\circ$ transitions, which is approximately 25 ns [29]; thus, we double this value and report that as the uncertainty in Δt. The third term in Eq. (1) is uncertainty in the streamwise velocity due to spanwise fluctuations in the x–y plane. This formulation is taken from Hill and Klewicki [36] and Bathel et al. [35]. To bound the error, the spanwise fluctuations v'_{RMS} are conservatively estimated to be 5% of

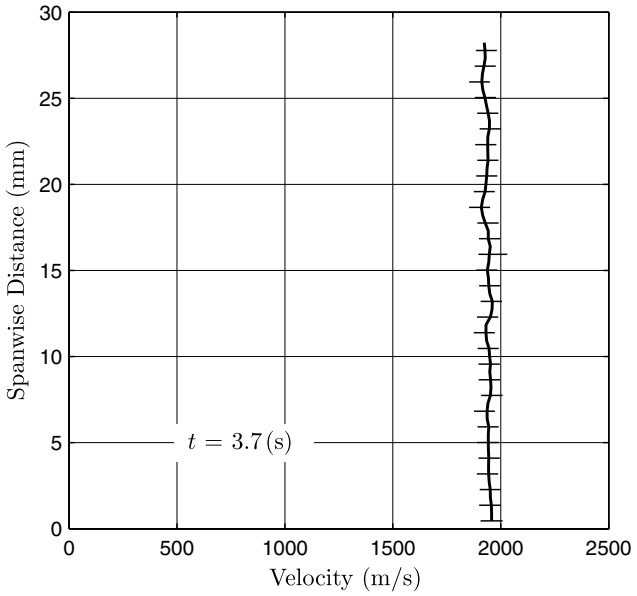

Fig. 5 Freestream-velocity profile for condition A. Error bars are horizontal thin black lines. The timestamp notes the time from camera trigger and is shared with Fig. 7, for reference.

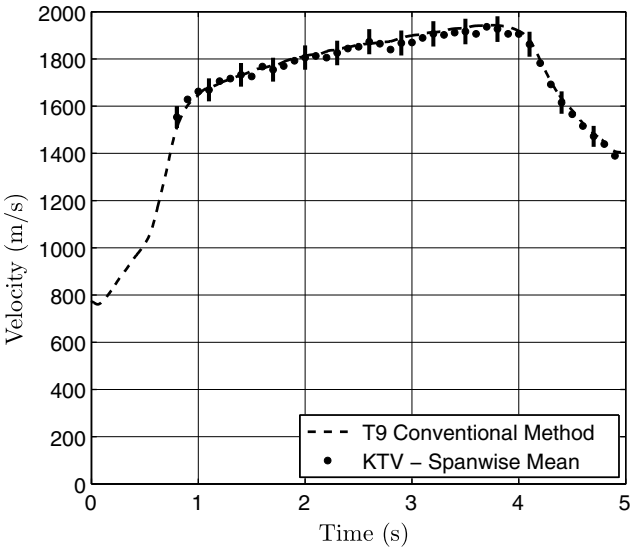

Fig. 7 Comparison of Tunnel 9 freestream velocity as calculated by conventional methods in Sec. III (dashed line) and measured by KTV (solid dots, spanwise average) vs time for condition A. Error bars are vertical thin black lines. The timestamp notes the time from camera trigger and is shared with Fig. 5.

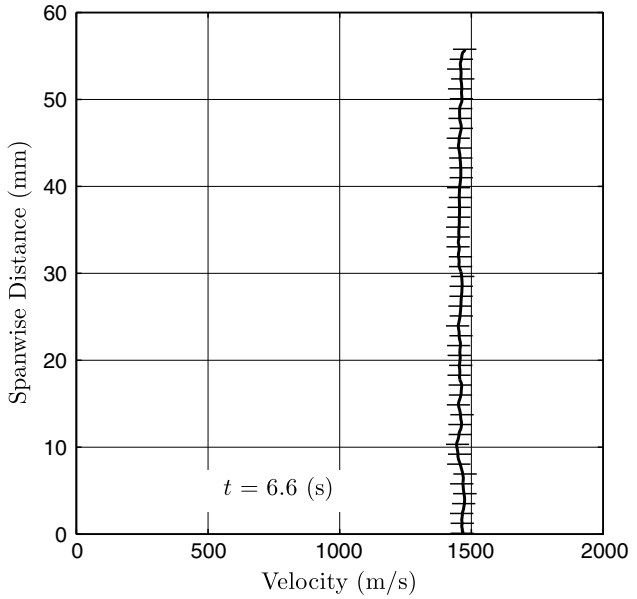

Fig. 6 Freestream-velocity profile for condition B. Error bars are horizontal thin black lines. The timestamp notes the time from camera trigger and is shared with Fig. 8, for reference.

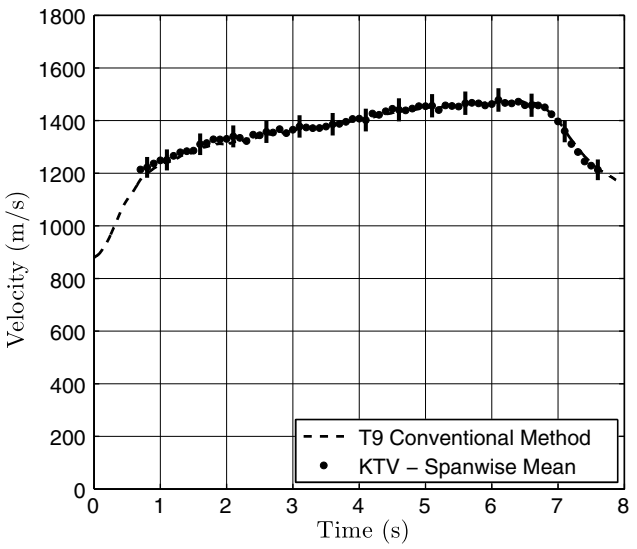

Fig. 8 Comparison of Tunnel 9 freestream velocity as calculated by conventional methods in Sec. III (dashed line) and measured by KTV (solid dots, spanwise average) vs time for condition B. Error bars are vertical thin black lines. The timestamp notes the time from camera trigger and is shared with Fig. 6.

the freestream velocity (v'_{RMS} is expected to be far lower in the Tunnel 9 freastream). The error in the KTV measurement is approximately 3% in the freestream, primarily due to the uncertainty in determining the line center and timing.

To characterize the flow uniformity in the measured field of view, the standard deviation of each profile was computed and normalized by the mean velocity. To search for trends, this was done for each time step for each condition. No trends were found in time or run condition, and the normalized standard deviation of the freestream-velocity profiles was observed to be in the range of 0.2–1.25%. This value is well within the uncertainty limits of the KTV technique as applied in this work.

In Figs. 7 and 8, we take the average of the profiles in Figs. 5, 6 in the spanwise direction and compare that to the freestream velocity value as calculated by conventional Tunnel 9 methods, detailed in Sec. III. The KTV data appear to match the Tunnel 9 calculations throughout the test time.

VI. Conclusions

The ability to make measurements of the freestream-velocity profiles with krypton tagging velocimetry (KTV) in Tunnel 9 is demonstrated for four conditions spanning the range of $M_\infty = 9.4$–13.2 and $Re_\infty^{\mathrm{unit}} = 1.6$–$30\ \mathrm{m}^{-1}$. KTV exposures are presented for each Tunnel 9 condition. For two conditions, instantaneous velocity profiles and a comparison of the freestream velocity as calculated by conventional methods and KTV are presented. Agreement between the KTV measurements and the Tunnel 9 calculations is good throughout the test time; the difference between the two results is approximately 2%, which is within the KTV uncertainty estimate of approximately 3%. This is a notable result because the Tunnel 9 freestream velocity calculations rely on pressure/temperature measurements and an appropriate treatment of the nonperfect gas nozzle expansion from the reservoir to the freestream; in contrast, the KTV profiles and traces represent a direct measurement. This provides a new experimental verification of the Tunnel 9 velocity calculation procedure. In this vein, KTV could be used to measure the freestream velocity as the Tunnel 9 parameter space is expanded, for example, if a new nozzle is developed. In addition, the standard deviation of the freestream-velocity profiles exhibits no clear trends through the test time or with run condition and fall within the range of 0.2–1.25%, which is within the KTV uncertainty estimate of approximately 3%.

It is suggested that KTV could be used in Tunnel 9 to measure velocity profiles on large-scale test articles. In the AEDC Mach 3 Calibration Tunnel, KTV was first used to make freestream measurements and then extended to the turbulent boundary layer on the nozzle wall [27] and a shock-wave/turbulent-boundary-layer interaction [28]. Tagging velocimetry signal-to-noise ratio (SNR) is reduced in regions of high shear, and applications in large-scale facilities are technically challenging; however, if one considers the relative ratio of SNR in the Mach 3 Calibration Tunnel freestream to that in turbulent shear layers [27,28] and extrapolates from the Tunnel 9 freestream SNR presented in this note, the authors are confident that there will be sufficient SNR for KTV application in regions of high shear in Tunnel 9 flows of varying Mach number and unit Reynolds number.

Acknowledgments

The facilities were supplied by the Arnold Engineering Development Complex (AEDC). M. A. Mustafa and N. J. Parziale were supported by the U.S. Air Force Office of Scientific Research (AFOSR) Young Investigator Research Program (grant FA9550-16-1-0262), and equipment for this work was supported by AFOSR Defense University Research Instrumentation Program (grant FA9550-15-1-0325), for both of which Ivett Leyva (AFOSR) is the Program Manager. Preliminary efforts crucial to the success of this work were supported by the U.S. Air Force Summer Faculty Fellowship Program, in which Mike Kendra (AFOSR) has been supportive of participation by Stevens Institute of Technology personnel. The authors would like to thank A. J. Spicer of AEDC White Oak for his technical assistance in making these measurements. In addition, we would like to acknowledge the encouragement of John Laffery and Dan Marren of AEDC White Oak.

References

[1] Candler, G. V., "Rate-Dependent Energetic Processes in Hypersonic Flows," *Progress in Aerospace Sciences*, Vol. 72, 2015, pp. 37–48. doi:10.1016/j.paerosci.2014.09.006

[2] Canupp, P. W., Candler, G. V., Perkins, J. N., and Ericksons, W., "Analysis of Hypersonic Nozzles Including Vibrational Nonequilibrium and Intermolecular Force Effects," *AIAA Journal*, Vol. 31, No. 7, 1993, pp. 1243–1249. doi:10.2514/3.49065

[3] Candler, G. V., "Hypersonic Nozzle Analysis Using an Excluded Volume Equation of State," *38th AIAA Thermophysics Conference*, AIAA Paper 2005-5202, June 2005. doi:10.2514/6.2005-5202

[4] Clemens, N. T., and Narayanaswamy, V., "Low-Frequency Unsteadiness of Shock Wave/Turbulent Boundary Layer Interactions," *Annual Review of Fluid Mechanics*, Vol. 46, 2014, pp. 469–492. doi:10.1146/annurev-fluid-010313-141346

[5] Haertig, J., Havermann, M., Rey, C., and George, A., "Particle Image Velocimetry in Mach 3.5 and 4.5 Shock-Tunnel Flows," *AIAA Journal*, Vol. 40, No. 6, 2002, pp. 1056–1060. doi:10.2514/2.1787

[6] Loth, E., "Compressibility and Rarefaction Effects on Drag of a Spherical Particle," *AIAA Journal*, Vol. 46, No. 9, 2008, pp. 2219–2228. doi:10.2514/1.28943

[7] Hsu, A. G., Srinivasan, R., Bowersox, R. D. W., and North, S. W., "Molecular Tagging Using Vibrationally Excited Nitric Oxide in an Underexpanded Jet Flowfield," *AIAA Journal*, Vol. 47, No. 11, 2009, pp. 2597–2604. doi:10.2514/1.39998

[8] Dam, N., Klein-Douwel, R. J. H., Sijtsema, N. M., and ter Meulen, J. J., "Nitric Oxide Flow Tagging in Unseeded Air," *Optics Letters*, Vol. 26, No. 1, 2001, pp. 36–38. doi:10.1364/OL.26.000036

[9] Miles, R., Cohen, C., Connors, J., Howard, P., Huang, S., Markovitz, E., and Russell, G., "Velocity Measurements by Vibrational Tagging and Fluorescent Probing of Oxygen," *Optics Letters*, Vol. 12, No. 11, 1987, pp. 861–863. doi:10.1364/OL.12.000861

[10] Michael, J. B., Edwards, M. R., Dogariu, A., and Miles, R. B., "Femtosecond Laser Electronic Excitation Tagging for Quantitative Velocity Imaging in Air," *Applied Optics*, Vol. 50, No. 26, 2011, pp. 5158–5162. doi:10.1364/AO.50.005158

[11] Jiang, N., Halls, B. R., Stauffer, H. U., Danehy, P. M., Gord, J. R., and Roy, S., "Selective Two-Photon Absorptive Resonance Femtosecond-Laser Electronic-Excitation Tagging Velocimetry," *Optics Letters*, Vol. 41, No. 10, 2016, pp. 2225–2228. doi:10.1364/OL.41.002225

[12] Jiang, N., Mance, J. G., Slipchenko, M. N., Felver, J. J., Stauffer, H. U., Yi, T., Danehy, P. M., and Roy, S., "Seedless Velocimetry at 100 kHz with Picosecond-Laser Electronic-Excitation Tagging," *Optics Letters*, Vol. 42, No. 2, 2017, pp. 239–242. doi:10.1364/OL.42.000239

[13] Jiang, N., Nishihara, M., and Lempert, W. R., "Quantitative NO_2 Molecular Tagging Velocimetry at 500 kHz Frame Rate," *Applied Physics Letters*, Vol. 97, No. 22, 2010, Paper 221103. doi:10.1063/1.3522654

[14] Bathel, B. F., Johansen, C. T., Danehy, P. M., Inman, J. A., and Jones, S. B., "Hypersonic Boundary Layer Transition Measurements Using $NO_2 \rightarrow NO_2$ Photo-dissociation Tagging Velocimetry," *Proceedings of 41st AIAA Fluid Dynamics Conference and Exhibit*, AIAA Paper- 2011-3246, 2011. doi:10.2514/6.2011-3246

[15] ElBaz, A. M., and Pitz, R. W., "N_2O Molecular Tagging Velocimetry," *Applied Physics B*, Vol. 106, No. 4, 2012, pp. 961–969. doi:10.1007/s00340-012-4872-5

[16] Balla, R. J., "Iodine Tagging Velocimetry in a Mach 10 Wake," *AIAA Journal*, Vol. 51, No. 7, 2013, pp. 1783–1786. doi:10.2514/1.J052416

[17] Lempert, W. R., Jiang, N., Sethuram, S., and Samimy, M., "Molecular Tagging Velocimetry Measurements in Supersonic Microjets," *AIAA Journal*, Vol. 40, No. 6, 2002, pp. 1065–1070. doi:10.2514/2.1789

[18] Boedeker, L. R., "Velocity Measurement by H_2O Photolysis and Laser-Induced Fluorescence of OH," *Optics Letters*, Vol. 14, No. 10, 1989, pp. 473–475. doi:10.1364/OL.14.000473

[19] Wehrmeyer, J. A., Ribarov, L. A., Oguss, D. A., and Pitz, R. W., "Flame Flow Tagging Velocimetry with 193-nm H_2O Photodissociation,"

Applied Optics, Vol. 38, No. 33, 1999, pp. 6912–6917.
doi:10.1364/AO.38.006912

[20] Pitz, R. W., Lahr, M. D., Douglas, Z. W., Wehrmeyer, J. A., Hu, S., Carter, C. D., Hsu, K.-Y., Lum, C., and Koochesfahani, M. M., "Hydroxyl Tagging Velocimetry in a Supersonic Flow over a Cavity," *Applied Optics*, Vol. 44, No. 31, 2005, pp. 6692–6700.
doi:10.1364/AO.44.006692

[21] André, M. A., Bardet, P. M., Burns, R. A., and Danehy, P. M., "Characterization of Hydroxyl Tagging Velocimetry for Low-Speed Flows," *Measurement Science and Technology*, Vol. 28, No. 8, 2017, Paper 085202.
doi:10.1088/1361-6501/aa7ac8

[22] Mills, J. L., Sukenik, C. I., and Balla, R. J., "Hypersonic Wake Diagnostics Using Laser Induced Fluorescence Techniques," *42nd AIAA Plasmadynamics and Lasers Conference*, AIAA Paper 2011-3459, June 2011.
doi:10.2514/6.2011-3459

[23] Balla, R. J., and Everhart, J. L., "Rayleigh Scattering Density Measurements, Cluster Theory, and Nucleation Calculations at Mach 10," *AIAA Journal*, Vol. 50, No. 3, 2012, pp. 698–707.
doi:10.2514/1.J051334

[24] Parziale, N. J., Smith, M. S., and Marineau, E. C., "Krypton Tagging Velocimetry for Use in High-Speed Ground-Test Facilities," *53rd AIAA Aerospace Sciences Meeting*, AIAA Paper 2015-1484, 2015.
doi:10.2514/6.2015-1484

[25] Parziale, N. J., Smith, M. S., and Marineau, E. C., "Krypton Tagging Velocimetry of an Underexpanded Jet," *Applied Optics*, Vol. 54, No. 16, 2015, pp. 5094–5101.
doi:10.1364/AO.54.005094

[26] Zahradka, D., Parziale, N. J., Smith, M. S., and Marineau, E. C., "Krypton Tagging Velocimetry (KTV) in Supersonic Turbulent Boundary Layers," *54th AIAA Aerospace Sciences Meeting*, AIAA Paper 2016-1587, 2016.
doi:10.2514/6.2016-1587

[27] Zahradka, D., Parziale, N. J., Smith, M. S., and Marineau, E. C., "Krypton Tagging Velocimetry in a Turbulent Mach 2.7 Boundary Layer," *Experiments in Fluids*, Vol. 57, No. 62, 2016.
doi:10.1007/s00348-016-2148-2

[28] Mustafa, M. A., Hunt, M. B., Parziale, N. J., Smith, M. S., and Marineau, E. C., "Krypton Tagging Velocimetry (KTV) Investigation of Shock-Wave/Turbulent Boundary-Layer Interaction," *55th AIAA Aerospace Sciences Meeting*, AIAA Paper 2017-0025, 2017.
doi:10.2514/6.2017-0025

[29] Chang, R. S. F., Horiguchi, H., and Setser, D. W., "Radiative Lifetimes and Two-Body Collisional Deactivation Rate Constants in Argon for Kr($4p^5 5p$) and Kr($4p^5 5p'$) States," *Journal of Chemical Physics*, Vol. 73, No. 2, 1980, pp. 778–790.
doi:10.1063/1.440185

[30] Marren, D., and Lafferty, J., "The AEDC Hypervelocity Wind Tunnel 9," *Advanced Hypersonic Test Facilities*, AIAA, Reston, VA, 2002, pp. 467–478.
doi:10.2514/5.9781600866678.0467.0478

[31] Goodwin, D. G., "An Open-Source, Extensible Software Suite for CVD Process Simulation," *Proceedings of CVD XVI and EuroCVD Fourteen*, edited by M. Allendorf, F. Maury, and F. Teyssandier, The Electrochemical Soc., Inc., Pennington, NJ, 2003, pp. 155–162.

[32] Chapman, S., and Cowling, T. G., *The Mathematical Theory of Non-Uniform Gases*, Cambridge Univ. Press, Cambridge, England, U.K., 1939, pp. 151–167.

[33] McBride, B. J., Zehe, M. J., and Gordon, S., "NASA Glenn Coefficients for Calculating Thermodynamic Properties of Individual Species," NASA TP-2002-211556, 2002.

[34] O'Haver, T., *A Pragmatic Introduction to Signal Processing*, Univ. of Maryland at College Park, College Park, MD, 1997, pp. 58–69.

[35] Bathel, B. F., Danehy, P. M., Inman, J. A., Jones, S. B., Ivey, C. B., and Goyne, C. P., "Velocity Profile Measurements in Hypersonic Flows Using Sequentially Imaged Fluorescence-Based Molecular Tagging," *AIAA Journal*, Vol. 49, No. 9, 2011, pp. 1883–1896.
doi:10.2514/1.J050722

[36] Hill, R. B., and Klewicki, J. C., "Data Reduction Methods for Flow Tagging Velocity Measurements," *Experiments in Fluids*, Vol. 20, No. 3, 1996, pp. 142–152.
doi:10.1007/BF00190270

J. M. Austin
Associate Editor